JOURNAL OF AGRICULTURAL AND FOOD CHEMISTRY

Bioactive Constituents, Metabolites, and Functions

Neolignan Constituents with Potential Beneficial Effects in Prevention of Type 2 Diabetes from Viburnum fordiae Hance Fruits

Chunchao Zhao, Jia Chen, Jianhua Shao, Jie Shen, Kehuan Li, Wenyan Gu, Sihui Li, and Judi Fan

J. Agric. Food Chem., **Just Accepted Manuscript** • DOI: 10.1021/acs.jafc.8b03772 • Publication Date (Web): 19 Sep 2018

ACS Publications

is published by the American Chemical Society. 1155 Sixteenth Street N.W., Washington, DC 20036

Neolignan Constituents with Potential Beneficial Effects in Prevention of Type 2 Diabetes from *Viburnum fordiae* Hance Fruits

Chunchao Zhao,[*,†,‡] Jia Chen,[†] Jianhua Shao,[*,†] Jie Shen,[†] Kehuan Li,[‡] Wenyan Gu,[‡] Sihui Li,[‡] and Judi Fan[§]

[†]Jiangsu Key Laboratory of Crop Genetics and Physiology/Co-Innovation Center for Modern Production Technology of Grain Crops, Yangzhou University, Yangzhou 225009, China

[‡]Joint International Research Laboratory of Agriculture & Agri-Product Safety of Ministry of Education of China, Yangzhou University, Yangzhou 225009, China

[§]School of Pharmacy, Guizhou Medical University, Guiyang 550004, China

[*] Corresponding authors. Tel: +86-514-87991556. E-mail: cczhao@yzu.edu.cn, jhshao@yzu.edu.cn.

ABSTRACT: Nine new neolignan glycosides (**1**−**9**), viburfordosides A−I, two new neolignans, fordianes A and B (**10**, **11**), and seven known analogues (**12**−**18**) have been isolated and identified from the fruits of *Viburnum fordiae* Hance. The structures and absolute configurations of undescribed neolignan constituents were identified by chemical methods and spectroscopic analyses. The α-glucosidase inhibitory, $ABTS^{\bullet+}$ and $DPPH^{\bullet}$ scavenging and anti-inflammatory activities of these secondary metabolites were evaluated. Some of them exhibited significant potency in inhibiting α-glucosidase and scavenging free radicals. Among fourteen metabolites that were found to have the capacity to inhibit NO production in LPS-stimulated RAW264.7 macrophage cells, compounds **2**, **4**, **6**, **10**, **11**, **14**, **17** and **18** were potent with IC_{50} values of 10.88 to 41.10 μM. These results support that *V. fordiae* fruits possessing the neolignan compounds may serve as both functional food and medicinal resource to prevent and treat type 2 diabetes (T2D).

KEYWORDS: Adoxaceae, *Viburnum fordiae* Hance, berry fruits, neolignans, α-glucosidase inhibition, radical scavenging, anti-inflammatory

INTRODUCTION

Type 2 diabetes (T2D), representing over 90% of diabetes, has reached pandemic proportions throughout the world, and is now recognized as a leading risk factor for cardiovascular events that are responsible for most of the deaths in diabetic patients, the proportion of which is up to 65%.[1–3] T2D is characterized by hyperglycemia. Prevention of hyperglycemia is important, especially following a meal when plasma glucose levels are highest.[1] Sustained postprandial hyperglycemia (PPHG) can result in postprandial oxidative stress and inflammation, and in turn, continued oxidative stress and inflammation in T2D mediate the action of acute hyperglycemia that is involved in the development of diabetes complications such as cardiovascular disease (CVD).[4–7]

Scientific evidence has revealed that PPHG can be effectively regulated by inhibiting carbohydrate-hydrolyzing enzymes to retard absorption of glucose.[8] Thus, α-glucosidase inhibitors, for example acarbose and miglitol, play a vital role in controlling T2D. However, their clinical application is limited due to their gastro-intestinal side effects and high cost.[9] Recently, more attention has been paid to plant-based foods, particularly some fruits and vegetables. In epidemiological research, the plant-based foods have been considered as the critical ingredients of dietary patterns that can effectively prevent chronic diseases such as T2D and CVD.[10,11] Polyphenols, abundant in fruits, vegetables and tea, have been reported to possess therapeutic potential in the management of T2D in humans.[12,13] These natural compounds have the inhibitory activity against α-glucosidase in concert with acarbose for effective glycemic control, and can provide protective effects on organs and tissues against oxidative stress and inflammation.[14–16] Therefore, some fruits and vegetables, especially berries, rich in polyphenols have been proposed for the prevention and treatment of T2D and CVD.

Viburnum fordiae Hance, also called "man shan hong" in Chinese due to its crimson berries, is distributed throughout South China region, particularly in mountain areas.[17] In recent years, the cultivation of *V. fordiae* is increasing in China due to its high economic values. Its stems, roots and leaves, known as traditional Chinese medicine, have been commonly used owing to their therapeutic efficacy in various inflammatory diseases.[17] And its fruits, containing large amounts of nutritional ingredients, such as vitamins, microelements and amino acids, are a type of edible berry, and usually used to make beverages in Jiangxi and Guizhou provinces, China.[18] Previous studies, including those from our group, have resulted in the identification of essential oils, terpenoids, neolignans and other phenolics from the stems, leaves and roots of *V. fordiae*, some of which exhibited weak or moderate antioxidant, anti-inflammatory and α-glucosidase inhibitory properties.[19−22] As an edible berry with abundant nutrient ingredients, the fruits of *V. fordiae* may be more suitable to be utilized as a food material than its stems, leaves and roots. However, to our knowledge, no investigations, involving biological activities and chemical components of *V. fordiae* fruits, have been reported. In our search for potential food materials for prevention of T2D, the *n*-butanol fraction from *V. fordiae* fruits showed significant α-glucosidase inhibitory, free radical scavenging and NO inhibitory activities. Therefore, it was subjected to phytochemical investigation and further bioactivity screening. In this paper, eleven undescribed neolignan constituents (**1**−**11**) and seven known analogues (**12**−**18**) from the fruits of *V. fordiae* were identified and their bioactivities were also evaluated *in vitro*.

MATERIALS AND METHODS

General Experimental Procedures. A JASCO (Tokyo, Japan) J-810 circular dichroism (CD) spectrometer, connected with Peltier temperature controller, was used to acquire CD data. A SGW-2

digital polarimeter (Yidian Wuli Guangxue Company, Shanghai, China) was used for experimental optical rotation measurements. UV–vis–NIR measurements were obtained by a Cary 5000 spectrophotometer (Varian, Palo Alto, USA). The Fourier transform infrared (FTIR) spectroscopy measurements were conducted using a 610/670 infrared microspectrometer (Varian, Palo Alto, USA), with the prepared powders diluted in KBr pellets. HR-ESIMS spectra were acquired by a UHR–TOF maxis instrument (Bruker, Bremen, Germany). A Bruker (Rheinstetten, Germany) Avance 600 MHz spectrometer was used to acquire 1D/2D NMR spectra.

Macroporous resin (HPD-100), ODS-A-HG, Sephadex LH-20, silica gel, and MCI-gel CHP20P applied to column chromatography (CC) were provided by Bonherb Technology Company (Hebei, China), YMC (Kyoto, Japan), GE Healthcare Biosciences (Uppsala, Sweden), Haiyang Chemical Company (Qingdao, China), and Mitsubishi Chemical Industries (Tokyo, Japan), respectively. β-Glucosidase, trolox, indomethacin, and acarbose were available from Sigma-Aldrich (St. Louis, USA). Semi-preparative HPLC was accomplished on a YMC-packed column (5 μm, 250 mm × 10 mm i.d.) with an LC3000 system (Chuangxin Tongheng Company, Beijing, China).

Plant Material. The fresh fruits of *V. fordiae*, used in this study, were picked in Guiyang city, Guizhou province, China, in October 2011. A voucher specimen (201102) was stored in Medicinal Plant Biotechnology Laboratory, Yangzhou University and identified by Professor Huyin Huai from Yangzhou University.

Extraction and Isolation. Air dried *V. fordiae* fruits (16.5 kg) were well mashed and then extracted with 95% ethanol three times. The extract was evaporated to obtain a residue. This residue was dissolved in distilled water, and then extracted in sequence with petroleum ether and *n*-butanol. The *n*-butanol part (830.0 g) was chromatographed over HPD-100 macroporous resin and orderly

eluted with H_2O and 95% ethanol to afford two portions. The 95% ethanol eluate (492.0 g) was loaded onto silica gel column with gradient solvents of MeOH/$CHCl_3$ (0:100 → 100:0) as the eluent, to acquire seven fractions (F_1–F_7).

Fraction F_2 was applied to the open column packed with MCI gel using the sequential elution with MeOH/H_2O (90:10) and acetone. The portion eluted by MeOH/H_2O (90:10) was applied to ODS CC using MeOH/H_2O (20:80 → 100:0) as the eluent, to yield six subfractions ($F_{2\text{-}1}$–$F_{2\text{-}6}$). $F_{2\text{-}2}$ was loaded onto Sephadex LH-20 column and eluted with MeOH/$CHCl_3$ (1:2) to give a mixture of compounds **15** and **16**. This mixture was fractionated by semi-prep. HPLC (MeOH/H_2O, 44:56, 1.5 mL/min) to produce compounds **15** (24 mg, t_R = 17.1 min) and **16** (10 mg, t_R = 21.1 min). $F_{2\text{-}3}$ was chromatographed over Sephadex LH-20 with MeOH/$CHCl_3$ (1:2) as the eluent, to yield compound **14** (58 mg) and a mixture, which was isolated by semi-prep. HPLC (MeOH/H_2O, 31:69, 1.5 mL/min) to give compounds **10** (178 mg, t_R = 67.4 min) and **11** (132 mg, t_R = 77.3 min). Another subfraction $F_{2\text{-}4}$ was applied to Sephadex LH-20 CC eluting with MeOH/$CHCl_3$ (1:2), and further separated by semi-prep. HPLC (MeOH/H_2O, 43:57, 1.5 mL/min), to obtain compounds **17** (11 mg, t_R = 71.1 min) and **18** (12 mg, t_R = 76.5 min).

Fraction F_5 was separated into six subfractions ($F_{5\text{-}1}$–$F_{5\text{-}6}$) through ODS CC eluting with MeOH/H_2O (5:95 → 100:0) and two consecutive Sephadex LH-20 CC with MeOH/$CHCl_3$ (1:2) and MeOH as the eluent, respectively. $F_{5\text{-}4}$ was applied to Sephadex LH-20 CC with MeOH/H_2O (45:55) as the eluent, to yield fractions $F_{5\text{-}4\text{-}1}$–$F_{5\text{-}4\text{-}4}$. $F_{5\text{-}4\text{-}2}$ was subjected to MCI gel CC using MeOH/H_2O (10:90 → 100:0) as the eluent, to yield fourteen fractions ($F_{5\text{-}4\text{-}2\text{-}1}$–$F_{5\text{-}4\text{-}2\text{-}14}$). $F_{5\text{-}4\text{-}2\text{-}6}$ was loaded onto Sephadex LH-20 column and eluted with MeOH, to give **1** (128 mg). $F_{5\text{-}4\text{-}2\text{-}7}$ was fractionated by Sephadex LH-20 CC eluting with MeOH, to give **5** (16 mg). $F_{5\text{-}4\text{-}2\text{-}9}$ was loaded onto Sephadex

LH-20 column using MeOH/$CHCl_3$ (1:2) as the eluent, to afford a mixture of **7**, **8**, **9**, and **12**. The mixture was separated by semi-prep. HPLC (MeOH/H_2O, 32:68, 1.5 mL/min) to give **7** (42 mg, t_R = 64.1 min), **8** (30 mg, t_R = 68.6 min), **9** (25 mg, t_R = 72.7 min), and **12** (15 mg, t_R = 66.0 min). $F_{5\text{-}4\text{-}2\text{-}11}$ was applied to Sephadex LH-20 CC with MeOH/$CHCl_3$ (1:2) as the eluent, to produce a mixture, which was fractionated by semi-prep. HPLC (MeOH/H_2O, 33:67, 1.5 mL/min) to yield **3** (12 mg, t_R = 84.4 min) and **2** (19 mg, t_R = 96.3 min). $F_{5\text{-}4\text{-}2\text{-}13}$ was fractionated by Sephadex LH-20 CC eluting with MeOH and then subjected to semi-prep. HPLC (MeOH/H_2O, 42:58, 1.5 mL/min) to give **4** (14 mg, t_R = 31.8 min) and **6** (21 mg, t_R = 35.7 min). Compound **13** (10 mg, t_R = 82.5 min) was acquired from $F_{5\text{-}4\text{-}3}$ on Sephadex LH-20 column eluting with MeOH, in combination with semi-prep. HPLC (MeOH/H_2O, 33:67, 1.5 mL/min).

*Viburfordoside A (**1**)*. White powder; HR-ESIMS *m/z* 735.2486 $[M + Na]^+$ (calcd for $C_{33}H_{44}O_{17}Na$, 735.2471); CD (MeOH) λ ($\Delta\varepsilon$) 216 (+2.02), 221 (–4.15), 234 (–7.38), 271 (+5.60) nm; UV (MeOH) λ_{max} (log ε) 208 (4.89), 274 (4.46) nm; $[\alpha]_D^{23}$ –24.0 (*c* 0.10, MeOH); 1D NMR data, Tables 1, 3; IR (KBr) ν_{max} 3401, 1599, 1498, 1463, 1127, 1074, 1022, 890, 636 cm^{-1}.

*Viburfordoside B (**2**)*. White powder; HR-ESIMS *m/z* 885.2795 $[M + Na]^+$ (calcd for $C_{41}H_{50}O_{20}Na$, 885.2788); CD (MeOH) λ ($\Delta\varepsilon$) 217 (–6.77), 235 (+4.35), 272 (–6.79) nm; UV (MeOH) λ_{max} (log ε) 213 (4.28), 268 (3.97) nm; $[\alpha]_D^{23}$ –50.4 (*c* 0.10, MeOH); 1D NMR data, Tables 1, 3; IR (KBr) ν_{max} 3400, 1703, 1598, 1500, 1463, 1123, 1072, 824, 765, 629 cm^{-1}.

*Viburfordoside C (**3**)*. White powder; HR-ESIMS *m/z* 915.2897 $[M + Na]^+$ (calcd for $C_{42}H_{52}O_{21}Na$, 915.2893); CD (MeOH) λ ($\Delta\varepsilon$) 235 (+8.96), 275 (–13.39) nm; UV (MeOH) λ_{max} (log ε) 276 (4.78) nm; $[\alpha]_D^{23}$ –16.2 (*c* 0.10, MeOH); 1D NMR data, Tables 1, 3; IR (KBr) ν_{max} 3406, 1704, 1600, 1499, 1462, 1120, 1073, 822, 765, 669 cm^{-1}.

131 *Viburfordoside D (**4**)*. White powder; HR-ESIMS *m/z* 885.2790 $[M + Na]^+$ (calcd for $C_{41}H_{50}O_{20}Na$,
132 885.2788); CD (MeOH) λ ($\Delta\varepsilon$) 224 (+3.99), 231 (+4.59), 277 (–12.28), 285 (–12.64) nm; UV
133 (MeOH) λ_{max} (log ε) 277 (4.64) nm; $[\alpha]_D^{23}$ –13.3 (*c* 0.10, MeOH); 1D NMR data, Tables 1, 3; IR (KBr)
134 ν_{max} 3391, 1706, 1605, 1513, 1463, 1114, 1074, 1030, 863, 765, 669 cm^{-1}.

135 *Viburfordoside E (**5**)*. White powder; HR-ESIMS *m/z* 707.2524 $[M + Na]^+$ (calcd for $C_{32}H_{44}O_{16}Na$,
136 707.2522); CD (MeOH) λ ($\Delta\varepsilon$) 241 (+2.58), 290 (+1.17) nm; UV (MeOH) λ_{max} (log ε) 282 (3.92) nm;
137 $[\alpha]_D^{23}$ +14.8 (*c* 0.10, MeOH); 1D NMR data, Tables 1, 3; IR (KBr) ν_{max} 3392, 1608, 1498, 1076, 1033,
138 897, 633 cm^{-1}.

139 *Viburfordoside F (**6**)*. White powder; HR-ESIMS *m/z* 857.2829 $[M + Na]^+$ (calcd for $C_{40}H_{50}O_{19}Na$,
140 857.2839); CD (MeOH) λ ($\Delta\varepsilon$) 218 (+2.49), 233 (–4.48), 277 (–2.17) nm; UV (MeOH) λ_{max} (log ε)
141 266 (4.45) nm; $[\alpha]_D^{23}$ –35.9 (*c* 0.10, MeOH); 1D NMR data, Tables 1, 3; IR (KBr) ν_{max} 3436, 1703,
142 1599, 1514, 1280, 1076, 1032, 856, 763 cm^{-1}.

143 *Viburfordoside G (**7**)*. White powder; HR-ESIMS *m/z* 575.2087 $[M + Na]^+$ (calcd for $C_{27}H_{36}O_{12}Na$,
144 575.2099); CD (MeOH) λ ($\Delta\varepsilon$) 208 (+1.79), 229 (–3.66), 253 (+0.55), 281 (–0.42) nm; UV (MeOH)
145 λ_{max} (log ε) 267 (4.11) nm; $[\alpha]_D^{23}$ –18.8 (*c* 0.10, MeOH); 1D NMR data, Tables 2, 4; IR (KBr) ν_{max}
146 3391, 1600, 1511, 1464, 1266, 1074, 1032, 899, 669 cm^{-1}.

147 *Viburfordoside H (**8**)*. White powder; HR-ESIMS *m/z* 575.2090 $[M + Na]^+$ (calcd for $C_{27}H_{36}O_{12}Na$,
148 575.2099); CD (MeOH) λ ($\Delta\varepsilon$) 236 (–1.66), 283 (+0.58) nm; UV (MeOH) λ_{max} (log ε) 266 (4.38) nm;
149 $[\alpha]_D^{23}$ –21.2 (*c* 0.10, MeOH); 1D NMR data, Tables 2, 4; IR (KBr) ν_{max} 3384, 1600, 1511, 1463, 1264,
150 1073, 1031, 897, 667 cm^{-1}.

151 *Viburfordoside I (**9**)*. White powder; HR-ESIMS *m/z* 575.2085 $[M + Na]^+$ (calcd for $C_{27}H_{36}O_{12}Na$,
152 575.2099); CD (MeOH) λ ($\Delta\varepsilon$) 215 (–4.60), 224 (+1.90), 279 (–1.75) nm; UV (MeOH) λ_{max} (log ε)

266 (4.11) nm; $[\alpha]_D^{23}$ –17.8 (*c* 0.10, MeOH); 1D NMR data, Tables 2, 4; IR (KBr) ν_{max} 3390, 1600, 1511, 1465, 1265, 1074,1030, 898, 668 cm^{-1}.

*Fordiane A (**10**)*. Yellow oil; HR-ESIMS *m*/*z* 397.1280 $[M + Na]^+$ (calcd for $C_{20}H_{22}O_7Na$, 397.1258); CD (MeOH) λ ($\Delta\varepsilon$) 212 (+2.13), 216 (–1.54), 224 (+0.82), 231 (+0.80) nm; UV (MeOH) λ_{max} (log ε) 226 (4.20), 337 (4.12) nm; $[\alpha]_D^{23}$ +38.5 (*c* 0.10, MeOH); 1D NMR data, Tables 2, 4; IR (KBr) ν_{max} 3391, 2939, 2839, 1662, 1596, 1510, 1465, 1272, 1135, 1031, 972, 815, 599 cm^{-1}.

*Fordiane B (**11**)*. Yellow oil; HR-ESIMS *m*/*z* 397.1257 $[M + Na]^+$ (calcd for $C_{20}H_{22}O_7Na$, 397.1258); CD (MeOH) λ ($\Delta\varepsilon$) 212 (–1.00), 217 (+0.39), 225 (–0.47), 235 (+0.32) nm; UV (MeOH) λ_{max} (log ε) 223 (3.91), 335 (3.95) nm; $[\alpha]_D^{23}$ –16.9 (*c* 0.10, MeOH); 1D NMR data, Tables 2, 4; IR (KBr) ν_{max} 3389, 2925, 2852, 1656, 1597, 1512, 1460, 1272, 1137, 1029, 814, 592 cm^{-1}.

Enzymatic Hydrolysis of 1, 5, 7−9, and 12. The enzymatic hydrolysis reaction was conducted in accordance with a previously reported method.[23] Briefly, at 37 °C for 12 or 24 h, compounds **1**, **5**, **7**−**9**, and **12** were separately hydrolyzed by β-glucosidase (10 mg) in H_2O (3 mL), and then extracted by EtOAc for three times. The EtOAc phases from **1**, **5**, **7**−**9**, and **12** were isolated and purified to give aglycones, **1a**, **5a**, **7a**−**9a** and **12a**, respectively. The aqueous phases were isolated and purified to obtain glucose possessing $[\alpha]_D$ values in range from +42.5 to +53.9 (*c* = 0.15 → 0.30, H_2O). The *n*-BuOH/CH_3COOH/H_2O(4:1:5) was used as developing solvent, and the glucose was identified by the paper chromatography with authentic D-glucose.

Acid Hydrolysis of 2−4 and 6. The acid hydrolysis reaction was performed in accordance with a previously reported method.[24] The EtOAc phases were isolated and purified by silica gel CC, using MeOH/$CHCl_3$ (1:8) as the eluent, for the hydrolyzates from **2** and **6** to yield vanillic acid, and from **3** and **4** to give syringic acid. These phenolic acids were confirmed by comparing with authentic

175 samples through Co-TLC, melting point and HPLC data. The aqueous phases of **2**−**4** and **6** were
176 identified according to the enzymatic hydrolysis method.

177 ***α*-Glucosidase Inhibitory Assay.** The assay for evaluating inhibitory ability of all isolates toward
178 α-glucosidase was set up as formerly reported.[25] The positive control used was acarbose. The
179 α-glucosidase inhibitory effect of tested compounds was qualified in terms of IC_{50} value, which
180 denoted the sample concentration demanded for exhibiting 50% of anti-α-glucosidase activity.

181 **Radical Scavenging Assay.** The $ABTS^{\bullet+}$ and $DPPH^{\bullet}$ assays of isolated compounds were
182 conducted in accordance with previously described.[26] The positive control used was trolox. The
183 calculated formula of radical scavenging activity (RSA) was determined as $RSA\%=[(OD_{control} -$
184 $OD_{sample})/(OD_{control} - OD_{blank})] \times 100$ %. The IC_{50} values represented the concentrations of tested
185 compounds in which 50% of $ABTS^{+}$ or DPPH radicals could be scavenged.

186 **LPS-Induced Nitric Oxide Production Inhibition Assay.** The measurement of NO in RAW264.7
187 cells was performed in accordance with a previously reported method using the Griess reaction.[27]
188 Nitrite levels in the supernatants were determined by comparing with the calibration curve prepared
189 with sodium nitrite standards. The positive control used in this assay was indomethacin. The nitric
190 oxide production inhibitory activity of the tested samples was determined as IC_{50} value.

191 **Statistical Analysis.** Each concentration of tested compounds was performed in triplicate. Data
192 from the experiments were described as the mean ± SD and evaluated with SPSS version 20.0. The
193 difference ($p < 0.05$) was statistically significant.

194 **RESULTS AND DISCUSSION**

195 **Identification of Compounds.** The *n*-butanol part from the 95% EtOH extract of *V. fordiae* fruits

196 was submitted to HPLC and other column chromatography through HPD-100 macroporous resin,
197 ODS, Sephadex LH-20, and MCI gel to afford eighteen different secondary metabolites. Compounds
198 **1**−**11** were identified as new compounds.

199 Viburfordoside A (**1**), white powder, had a molecular formula $C_{33}H_{44}O_{17}$ by positive HR-ESIMS.
200 Hydrolysis of **1** with *β*-glucosidase produced D-glucose with $[\alpha]_D^{23}$ = +48.6 (*c* 0.20, H_2O). The ^1H
201 NMR spectrum of **1** suggested the presence of two 1,3,4,5-tetrasubstituted benzene rings [δ_H 6.97
202 (br.s, H-2', 6') and 6.68 (s, H-2, 6)]. Two C3-units at C-7, -8, -9 [δ_H 5.50 (d, *J* = 6.6 Hz, H-7), 3.50 (m,
203 H-8), 3.66 (m, H-9b), 3.75 (m, H-9a)] and C-7', -8', -9' [δ_H 6.57 (d, *J* = 15.9 Hz, H-7'), 6.22 (dt, *J* =
204 15.9, 6.0 Hz, H-8'), 4.18 (dd, *J* = 13.6, 6.0 Hz, H-9'b), 4.40 (dd, *J* = 13.6, 6.0 Hz, H-9'a)] were
205 determined according to ^1H-^1H COSY and HSQC-TOCSY correlations (Figure 2). The ^1H NMR data
206 of **1** were closely identical to those of compound **13** except for signals of a glucose group and a
207 methoxyl residue. In the HMBC spectrum (Figure 2), the cross peaks from H-1''' (δ_H 4.91) to C-4 (δ_C
208 134.2) and H-1'' (δ_H 4.21) to C-9' (δ_C 68.7) showed that the linkage points of two glucose moieties
209 were at C-4 and C-9', respectively. Additionally, the HMBC cross peaks between three methoxy
210 protons and C-5/C-3/C-3' were observed. Consequently, **1** was confirmed to be
211 5-methoxydehydrodiconiferyl alcohol 4,9'-di-*O*-*β*-D-glucopyranoside. Because of the coupling
212 constant ($J_{7,8}$ = 6.6 Hz) of H-7 and H-8, the relative configuration of H-7 and H-8 of **1** was identified
213 as *trans*-form.[28] This was also confirmed by the cross peaks between H-7 and H-9, as well as
214 between H-2/H-6 and H-8 in the NOESY spectrum. The absolute configuration of **1** was confirmed
215 to be 7*S*, 8*R* by a positive Cotton effect near 271 nm in the CD spectrum.[29] Thus, viburfordoside A
216 was elucidated to have the structural formula **1** as shown in Figure 1.

217 The molecular formula $C_{41}H_{50}O_{20}$ of viburfordoside B (**2**) was exhibited in positive HR-ESIMS.

Acid hydrolysis of **2** produced two D-glucose groups with positive optical rotations. The β-anomer of D-glucose was confirmed by the coupling constant (J = 7.8 Hz or 6.8 Hz).[30] The 1D NMR spectra of **2** exhibited good similarity to those of **1** except for signals of a vanilloyl moiety. Comparison of the ^{13}C NMR data of **1** and **2** showed that the glucosyl C-6''' of **2** was characterized by a 2.7 ppm downfield shift, which suggested that the vanilloyl group was linked to C-6''' of **2**. This was also confirmed by the HMBC cross peaks between H-6''' (δ_H 4.45, 4.15) and C-7'''' (δ_C 165.4). The relative configuration of H-7 and H-8 of **2** was implied as *trans* form by the coupling constant ($J_{7,8}$ = 6.7 Hz) and the NOESY cross peaks from H-8 (δ_H 3.45) to H-2/H-6 (δ_H 6.64/6.64), and from H-9 (δ_H 3.73, 3.65) to H-7 (δ_H 5.49). Meanwhile, a negative Cotton effect near 272 nm indicated that the absolute configuration of **2** was determined as 7*R*, 8*S*.[26] Therefore, viburfordoside B was unambiguously confirmed to have the structural formula **2** as shown in Figure 1.

Viburfordoside C (**3**), white powder, had a molecular formula $C_{42}H_{52}O_{21}$ by positive HR-ESIMS. The 1D NMR signals of **3** were close to those of **2** except that the NMR signals of a vanilloyl moiety in **2** were replaced by those attributed to a syringoyl unit in **3**. This was also confirmed by HMBC cross peaks from H-1''' (δ_H 4.89) to C-4 (δ_C 134.1), from H-1'' (δ_H 4.21) to C-9' (δ_C 68.7), from H-6''' (δ_H 4.47, 4.19) to C-7'''' (δ_C 165.4), and from an additional OC$\underline{H}_3$ (δ_H 3.76) to C-5'''' (δ_C 147.5). A *trans* configuration of H-7 and H-8 of **3** was determined by the $J_{7,8}$ (6.5 Hz) and the NOESY cross peaks from H-8 (δ_H 3.41) to H-2/H-6 (δ_H 6.63/6.63), and from H-9 (δ_H 3.71, 3.65) to H-7 (δ_H 5.47). A negative Cotton effect near 275 nm showed that **3** could be identified as 7*R*, 8*S* configuration. Consequently, viburfordoside C was identified to have the structural formula **3** as shown in Figure 1.

Viburfordoside D (**4**), white powder, was assigned a molecular formula $C_{41}H_{50}O_{20}$ by positive HR-ESIMS. The NMR spectroscopic features of **4** were close to those of **3**, except that the NMR

signals of a 1,3,4,5-tetrasubstitued aromatic ring in **3** were replaced by those attributed to a 1,3,4-trisubstituted aromatic ring in **4**. This was further confirmed by HMBC cross peaks between H-1''' (δ_H 4.96) and C-4 (δ_C 146.1), H-1'' (δ_H 4.21) and C-9' (δ_C 68.7), H-6''' (δ_H 4.57, 4.19) and C-7'''' (δ_C 165.5), together with H-5 (δ_H 7.06) and C-1 (δ_C 135.3). The $J_{7,8}$ (6.1 Hz), the NOESY cross peaks from H-8 (δ_H 3.37) to H-2/H-6 (δ_H 6.95/6.67), and the negative Cotton effects at 277 and 285 nm showed that compound **4** possessed 7*R*, 8*S* configurations at C-7 and C-8. Thus, viburfordoside D was established to have the structural formula **4** as shown in Figure 1.

Viburfordoside E (**5**), white powder, was given a molecular formula of $C_{32}H_{44}O_{16}$ based on positive HR-ESIMS. The 1D NMR spectra of **5** were similar to those of glochidioboside[31] except for a set of glucosyl signals. The HMBC cross peak between H-1''' (δ_H 4.24) and C-9 (δ_C 70.1) showed that a glucose group was linked to C-9. Additionally, the HMBC cross peak between H-1'' (δ_H 4.12) and C-9' (δ_C 68.0) established that the other glucose group was attached to C-9'. The $J_{7,8}$ (7.1 Hz), the NOESY cross peak from H-8 (δ_H 3.58) to H-2 (δ_H 6.97), and a positive Cotton effect at 290 nm indicated that viburfordoside E was concluded to have the structural formula **5** as shown in Figure 1.

The molecular formula of viburfordoside F (**6**) was deduced to be $C_{40}H_{50}O_{19}$ by positive HR-ESIMS. The 1D NMR signals of **6** exhibited similarity with those of **5** except for signals of a vanillic acid moiety. By comparing the ^{13}C NMR data of **5** and **6**, the upfield shifts of the C-4 ($\Delta\delta$ 0.3) and C-9 ($\Delta\delta$ 7.1), and the downfield shifts of C-1 ($\Delta\delta$ 3.6) and C-6''' ($\Delta\delta$ 2.8) were observed in **6**. This indicated that two glucopyranosyl moieties were located at C-4 and C-9', and a vanilloyl moiety was linked to C-6''', which was also confirmed by the HMBC cross peaks from H-1''' (δ_H 4.97) to C-4 (δ_C 146.0), from H-1'' (δ_H 4.11) to C-9' (δ_C 67.9), and from H-6''' (δ_H 4.55, 4.16) to C-7'''' (δ_C 165.4). The $J_{7,8}$ (6.4 Hz), the NOESY cross peaks of H-2/H-6 (δ_H 6.96/6.75) and H-8 (δ_H 3.37), and a

262 negative Cotton effect near 277 nm suggested that **6** could be confirmed as 7*R*,8*S*-configuration.
263 Consequently, viburfordoside F was defined to have the structural formula **6** as shown in Figure 1.

264 Viburfordoside G (**7**), white powder, was given a molecular formula $C_{27}H_{36}O_{12}$ by positive
265 HR-ESIMS. Hydrolysis of **7** with *β*-glucosidase yielded **7a** and D-glucose. **7** exhibited NMR
266 spectroscopic data almost identical to those of glehlinoside H (**12**). A small coupling constant ($J_{7,8}$ =
267 4.7 Hz) was observed in the ^{1}H NMR spectrum of **7a** (Table S98), thus the relative configuration of
268 H-7 and H-8 of **7a** was determined as the *erythro*-form.[32] In the ^{13}C NMR spectrum, $\Delta\delta_{C8-C7}$ value of
269 **7** (12.0) was smaller than those of **8** (13.0) and **9** (13.0), which suggested that **7** should possess a
270 relative stereochemistry of 7,8-*erythro*, while **8** and **9** should be determined to be in the *threo*-form.[33]
271 The *R* configuration at C-8 of **7** was confirmed by a negative Cotton effect near 229 nm.[34] Thus,
272 viburfordoside G was determined to have the structural formula **7** in Figure 1.

273 The spectroscopic data of viburfordoside H (**8**) (Tables 2 and 4) indicated that it was a
274 *threo*-isomer of **7**. Hydrolysis of **8** with *β*-glucosidase gave D-glucose and **8a**. A large coupling
275 constant $J_{7,8}$ = 8.0 Hz, in the ^{1}H NMR spectrum of **8a** (Table S98), showed that the relative
276 configuration of **8a** was assigned as the *threo*-form of H-7 and H-8.[32] A negative Cotton effect near
277 236 nm demonstrated that the absolute configuration of **8** was 7*R*, 8*R* as shown in Figure 1.

278 Viburfordoside I (**9**) showed spectroscopic data (Tables 2 and 4) completely identical to those of **8**.
279 However, **8** and **9** were fractionated by semi-prep. HPLC with retention times of 68.6 min and 72.7
280 min, respectively. Hydrolysis of **9** with *β*-glucosidase yielded **9a** and D-glucose. The $J_{7,8}$ (J = 8.0 Hz)
281 (Table S98) of the aglycone (**9a**) and a positive Cotton effect near 224 nm of **9** showed that the
282 absolute configuration of viburfordoside I was identified to be 7*S*, 8*S* as shown in Figure 1.

283 Fordiane A (**10**), yellow oil, was assigned a molecular formula $C_{20}H_{22}O_7$ by positive HR-ESIMS.

In the ^{1}H NMR spectrum of **10** (Tables 2 and 4), besides two sets of ABX proton signals, an aldehyde signal at δ_H 9.60 (d, J = 7.8 Hz, H-9') and *trans*-olefinic protons at δ_H 6.76 (dd, J = 15.8, 7.8 Hz, H-8'), 7.60 (d, J = 15.8 Hz, H-7') established the presence of a *trans*-propenal group. And a 1,2,3-propanetriol moiety was confirmed by two oxymethine protons at δ_H 4.47 (m, H-8) and 4.70 (t-like, J = 5.0 Hz, H-7), as well as two oxymethylene protons at δ_H 3.62 (m, H-9b) and 3.65 (m, H-9a). The HMBC cross peak between H-8 (δ_H 4.47) and C-4' (δ_C 151.2) indicated that the aryl glycerol-8-yloxy was linked to C-4'. The above evidence indicated that **10** had the same planar structure as guaiacylglycerol-β-coniferyl aldehyde ether.[35] However, guaiacylglycerol-β-coniferyl aldehyde ether, with relative configuration determined, was reported to have ambiguous absolute configuration.[35,36] The *erythro*-form of H-7 and H-8 in **10** was identified by a small coupling constant ($J_{7,8}$ = 5.0 Hz, in $CDCl_3$, Table S98). Furthermore, a positive Cotton effect near 231 nm showed that **10** had a *S* configuration at C-8. Thus, fordiane A was delineated to have the structural formula **10** as shown in Figure 1.

The spectroscopic data of fordiane B (**11**) (Tables 2 and 4) indicated that it was a *threo*-isomer of **10**. A large coupling constant ($J_{7,8}$ = 7.7 Hz, in $CDCl_3$, Table S98) showed that **11** had the *threo*-form of H-7 and H-8. Meanwhile, a positive Cotton effect near 235 nm indicated that **11** possessed the 7*S*, 8*S* configuration. Consequently, fordiane B was defined to have the structural formula **11** as shown in Figure 1.

The other compounds were confirmed as glehlinoside H (**12**),[37] dehydrodiconiferyl alcohol 9'-*O*-β-D-glucopyranoside (**13**),[38] (7*S*,8*R*)-4,9'-dihydroxyl-3,3'-dimethoxyl-7,8-dihydrobenzofuran-1'-propylneolignan (**14**),[39] (7*R*,8*S*)-guaiacylglycerol-8-*O*-4'-(synapyl alcohol) ether (**15**),[40,41]

306 (7*S*,8*S*)-guaiacylglycerol-8-*O*-4'-(synapyl alcohol) ether (**16**),[41] lappaol A (**17**),[42] and isolappaol A
307 (**18**).[42]

308 ***α*-Glucosidase Inhibitory Activity.** All isolates were assayed for intestinal *α*-glucosidase
309 inhibitory activity. In comparison with positive control, these compounds exhibited potential
310 inhibitory activity toward *α*-glucosidase (Table 5). Among them, **10** and **11** demonstrated the most
311 potent inhibitory activity toward *α*-glucosidase (IC_{50} = 14.17 and 15.56 μM, respectively). The IC_{50}
312 values obtained showed that it was indefinite to discover the obvious differences in the structure–
313 activity relationships of 4',7-epoxy-8,5'-neolignan constituents, however, it was easy to find out that
314 the changes in configurations at C-7/C-8 of compounds **7**−**9**, **12** were of negligible importance in
315 inhibiting intestinal *α*-glucosidase activity.

316 **Free Radical Scavenging Activity.** Eighteen different secondary metabolites were assayed for
317 free radical scavenging activities. The tested compounds exhibited varying $ABTS^{\bullet+}$ and $DPPH^{\bullet}$
318 scavenging activities except compounds **1**, **7**−**9** and **12** as shown in Table 5. These obtained results
319 showed the fact that the free phenolic hydroxyl played a key role in free radical scavenging
320 activities.[43] Additionally, comparing with the $DPPH^{\bullet}$ assay, the $ABTS^{\bullet+}$ assay was significantly
321 powerful for fruits, which was consistent with the previous report.[44] Compounds **10** and **11**
322 demonstrated potent $ABTS^{\bullet+}$ scavenging activities (IC_{50} = 10.80 and 18.65 μM, respectively), which
323 were stronger than trolox (IC_{50} = 26.30 μM). In the $DPPH^{\bullet}$ assay, the IC_{50} values of compounds **10**
324 and **11** were 17.98 and 30.56 μM, respectively, which were comparable to that of trolox (IC_{50} = 38.68
325 μM). Interestingly, among 8,4'-oxyneolignan stereoisomers, compound **11** (7*S*) was weaker than **10**
326 (7*R*), and **16** (7*S*) was weaker than **15** (7*R*) in ABTS and DPPH radical scavenging tests, which
327 implied that *R* configuration at C-7 of these compounds may play a key role in exerting free radical

scavenging activity. Meanwhile, the weak activity of compounds **1**−**9**, **12**, and **13** indicated that the reduction of the radical scavenging effect may be correlated to glycosylation.

Inhibitory Effects on LPS-induced NO Production. All isolates were examined for their cytotoxic activity on RAW264.7 macrophage cells by the MTT assay and showed no toxicity at the dose evaluated (100 μM), and then assayed for the inhibition on LPS-induced NO production. Compounds **2**−**12**, **14**, **17** and **18** exhibited differential inhibitory effects against NO production (IC_{50} = 10.88 → 90.43 μM) in comparison with indomethacin (IC_{50} = 49.46 μM) (Table 5), and among which, **10**, **11** and **14** exhibited the strongest inhibitory effect with IC_{50} values of 10.88, 15.50 and 12.54 μM, respectively. Comparing with compounds **1** and **5**, an additional vanilloyl or syringoyl moiety in compounds **2**−**4** and **6**, located at C-6''' of glucosyl group appeared to reduce LPS-induced NO production. Compound **5** exhibited significantly weaker inhibitory effect on NO production than **14**, which attributed to two additional bulky glucose moieties in **5**. Similarly, comparing **3** (IC_{50} = 54.43 μM) with **2** (IC_{50} = 41.10 μM) and **4** (IC_{50} = 39.38 μM), an additional methoxyl group located at C-5 or C-5'''' could clearly reduce the inhibitory effect on NO production.

In conclusion, our research resulted in eleven undescribed neolignan constituents (**1**−**11**) and seven known analogues (**12**−**18**) isolated from *V. fordiae* fruits. Among these secondary metabolites, new compounds **2**−**4** and **6** are unusual 4',7-epoxy-8,5'-neolignan glycosides with a phenolic glucosyl group. The neolignan constituents are firstly reported from the edible fruits of *Viburnum* species. In bioactivity screening, these neolignans exhibited various α-glucosidase inhibitory, free radical scavenging and NO inhibitory activities. Interestingly, relative to the other tested neolignans, compounds **10** and **11** exhibited the most potent bioactivities in all three assays, which was probably associated with α, β-unsaturated aldehyde group in their structures. Therefore, these research results

not only revealed that the neolignans were major bioactive constituents of *V. fordiae* fruits, but also supported the edible berry of *V. fordiae* as functional food source for prevention of PPHG. Moreover, two new neolignans **10** and **11**, because of their potent bioactivities, may be developed as natural health-promoting food ingredients or further act as potential lead molecules for development of therapeutic agents for T2D.

ASSOCIATED CONTENT

Supporting Information

HR-ESIMS, IR, UV, CD, 1D/2D NMR spectra for **1**−**11**, ^{1}H NMR spectra for **7a**−**9a**, ORD values of **7a**–**9a**, **12a**.

AUTHOR INFORMATION

Corresponding Authors

* E-mail: cczhao@yzu.edu.cn.

* E-mail: jhshao@yzu.edu.cn.

ORCID

Chunchao Zhao: 0000-0001-7941-8175

Jianhua Shao: 0000-0003-2519-6735

Funding

This work was funded by National Natural Science Foundation of China (31201563).

Notes

The authors declare no competing financial interest.

ACKNOWLEDGMENTS

We thank Dr. Fengmin Zhang, Dr. Qiuxiang Yan and Dr. Chunliang Lu from Yangzhou University for spectroscopic tests.

REFERENCES

(1) Borror, A.; Zieff, G.; Battaglini, C.; Stoner, L. The effects of postprandial exercise on glucose control in individuals with type 2 diabetes: A systematic review. *Sports Med*. **2018**, *48*, 1479–1491.

(2) King, H.; Aubert, R. E.; Herman, W. H. Global burden of diabetes, 1995–2025: Prevalence, numerical estimates, and projections. *Diabetes Care* **1998**, *21*, 1414–1431.

(3) Nunes, S.; Rolo, A. P.; Palmeira, C. M.; Reis, F. Diabetic cardiomyopathy: Focus on oxidative stress, mitochondrial dysfunction and inflammation. In *Cardiomyopathies-Types and Treatments*. InTech publidsher: London, 2017; pp 235–257.

(4) Aparna, P.; Tiwari, A. K.; Srinivas, P. V.; Ali, A. Z.; Anuradha, V.; Rao, J. M. Dolichandroside A, a new α-glucosidase inhibitor and DPPH free-radical scavenger from *Dolichandrone falcata* Seem. *Phytother. Res*. **2009**, *23*, 591–596.

(5) Fukaya, N.; Mochizuki, K.; Shimada, M.; Goda, T. The α-glucosidase inhibitor miglitol decreases glucose fluctuations and gene expression of inflammatory cytokines induced by hyperglycemia in peripheral leukocytes. *Nutrition* **2009**, *25*, 657–667.

(6) Ceriello, A.; Assaloni, R.; Da Ros, R.; Maier, A.; Piconi, L.; Quagliaro, L.; Esposito, K.; Giugliano, D. Effect of atorvastatin and irbesartan, alone and in combination, on postprandial endothelial dysfunction, oxidative stress, and inflammation in type 2 diabetic patients. *Circulation* **2005**, *111*, 2518–2524.

(7) Ceriello, A. Postprandial hyperglycemia and diabetes complications: Is it time to treat? *Diabetes* **2005**, *54*, 1–7.

(8) Tundis, R.; Loizzo, M. R.; Menichini, F. Natural products as *α*-amylase and *α*-glucosidase inhibitors and their hypoglycaemic potential in the treatment of diabetes: An update. *Mini-Rev. Med. Chem*. **2010**, *10*, 315–331.

(9) Bellesia, A.; Tagliazucchi, D. Cocoa brew inhibits *in vitro α*-glucosidase activity: The role of polyphenols and high molecular weight compounds. *Food Res. Int.* **2014**, *63*, 439–445.

(10) Burton-Freeman, B. Postprandial metabolic events and fruit-derived phenolics: A review of the science. *Br. J. Nutr*. **2010**, *104*, S1–S14.

(11) Xi, P.; Liu, R. H. Whole food approach for type 2 diabetes prevention. *Mol. Nutr. Food Res.* **2016**, *60*, 1819–1836.

(12) Guasch-Ferré, M.; Merino, J.; Sun, Q.; Fitó, M.; Salas-Salvadó, J. Dietary polyphenols, mediterranean diet, prediabetes, and type 2 diabetes: A narrative review of the evidence. *Oxid. Med. Cell. Longev*. **2017**, available at https://doi.org/10.1155/2017/6723931.

(13) Vitale, M.; Vaccaro, O.; Masulli, M.; Bonora, E.; Del Prato, S.; Giorda, C. B.; Nicolucci, A.; Squatrito, S.; Auciello, S.; Babini, A. C.; et al. Polyphenol intake and cardiovascular risk factors in a population with type 2 diabetes: The TOSCA.IT study. *Clin. Nutr.* **2017**, *36*, 1686–1692.

(14) McDougall, G. J.; Shpiro, F.; Dobson, P.; Smith, P.; Blake, A.; Stewart, D. Different polyphenolic components of soft fruits inhibit *α*-amylase and *α*-glucosidase. *J. Agric. Food Chem.* **2005**, *53*, 2760–2766.

(15) Hwang, S. J.; Yoon, W. B.; Lee, O. H.; Cha, S. J.; Kim, J. D. Radical-scavenging-linked antioxidant activities of extracts from black chokeberry and blueberry cultivated in Korea. *Food*

Chem. **2014**, *146*, 71–77.

(16) Rahman, I.; Biswas, S. K.; Kirkham, P. A. Regulation of inflammation and redox signaling by dietary polyphenols. *Biochem. Pharmacol*. **2006**, *72*, 1439–1452.

(17) Zhonghuabencao Editorial Board. In *Zhonghuabencao*; Shanghai Scientific and Technical Press: Shanghai, China, 1999; Vol. 20, pp 553–554.

(18) Shao, Z. X.; Liu, A. Q.; Lu, B.; Yao, J. Z. Exploitation and utilization on *Viburnum* plants in Yunnan. *Chin. Wild Plant* **1992**, *11*, 29–31.

(19) Shao, J. H.; Chen, J.; Zhao, C. C.; Shen, J.; Liu, W. Y.; Gu, W. Y.; Li, K. H. Insecticidal and α-glucosidase inhibitory activities of chemical constituents from *Viburnum fordiae* Hance. *Nat. Prod. Res.* **2018**, available at https://doi.org/10.1080/14786419.2018.1466130.

(20) Chen, J.; Shao, J. H.; Zhao, C. C.; Shen, J.; Dong, Z. L.; Liu, W. Y.; Zhao, M.; Fan, J. D. Chemical constituents from *Viburnum fordiae* Hance and their anti-inflammatory and antioxidant activities. *Arch. Pharm. Res.* **2018**, *41*, 625–632.

(21) Wu, B.; Zheng, X. T.; Qu, H. B.; Cheng, Y. Y. Phenolic glycosides from *Viburnum fordiae* Hance and their antioxidant activities. *Lett. Org. Chem.* **2008**, *5*, 324−327.

(22) Zhu, X. Y.; Lu, R. M.; Lu, G. Z.; Zhao, H. Y. Analysis of chemical constituents of essential oils from *Viburnum fordiae* by GC-MS. *Lishizhen Med. Mater. Med. Res.* **2011**, *22*, 2101–2102.

(23) Jiang, Y. P.; Liu, Y. F.; Guo, Q. L.; Jiang, Z. B.; Xu, C. B.; Zhu, C. G.; Yang, Y. C.; Lin, S.; Shi, J. G. C_{14}-polyacetylene glucosides from *Codonopsis pilosula*. *J. Asian Nat. Prod. Res.* **2015**, *17*, 601−614.

(24) Yang, Y. N.; Liu, Z. Z.; Feng, Z. M.; Jiang, J. S.; Zhang, P. C. Lignans from the root of *Rhodiola crenulata*. *J. Agric. Food Chem.* **2012**, *60*, 964−972.

435 (25) Zhao, C. C.; Chen, J.; Shao, J. H.; Shen, J.; Xu, X. Q.; Li, K. H.; Gu, W. Y.; Zhao, M.; Fan, J.
436 D. Isolation of neolignan and phenolic glycosides from the branches of *Viburnum macrocephalum* f.
437 *keteleeri* and their *α*-glucosidase inhibitory activity. *Holzforschung* **2018**, available at
438 https://doi.org/10.1515/hf-2018-0081.
439 (26) Liu, Q. B.; Huang, X. X.; Bai, M.; Chang, X. B.; Yan, X. J.; Zhu, T.; Zhao, W.; Peng, Y.; Song,
440 S. J. Antioxidant and anti-inflammatory active dihydrobenzofuran neolignans from the seeds of
441 *Prunus tomentosa*. *J. Agric. Food Chem.* **2014**, *62*, 7796−7803.
442 (27) Xiang, L. M.; Wang, Y. H.; Yi, X. M.; He, X. J. Antiproliferative and anti-inflammatory
443 furostanol saponins from the rhizomes of *Tupistra chinensis*. *Steroids* **2016**, *116*, 28−37.
444 (28) Li, S.; Iliefski, T.; Lundquist, K.; Wallis, A. F. A. Reassignment of relative stereochemistry at
445 C-7 and C-8 in arylcoumaran neolignans. *Phytochemistry* **1997**, *46*, 929−934.
446 (29) Xiao, H. H.; Dai, Y.; Wong, M. S.; Yao, X. S. New lignans from the bioactive fraction of
447 *Sambucus williamsii* Hance and proliferation activities on osteoblastic-like UMR106 cells.
448 *Fitoterapia* **2014**, *94*, 29−35.
449 (30) Hudson, C. S.; Dale, J. K. Studies on the forms of *d*-glucose and their mutarotation. *J. Am.*
450 *Chem. Soc.* **1917**, *39*, 320−328.
451 (31) Takeda, Y.; Mima, C.; Masuda, T.; Hirata, E.; Takushi, A.; Otsuka, H. Glochidioboside, a
452 glucoside of (7*S*, 8*R*)-dihydrodehydrodiconiferyl alcohol from leaves of *Glochidion obovatum*.
453 *Phytochemistry* **1998**, *49*, 2137−2139.
454 (32) Besombes, S.; Robert, D.; Utille, J. P.; Taravel, F. R.; Mazeau, K. Molecular modeling of
455 syringyl and *p*-hydroxyphenyl *β*-*O*-4 dimers. Comparative study of the computed and experimental
456 conformational properties of lignin *β*-*O*-4 model compounds. *J. Agric. Food Chem.* **2003**, *51*, 34−42.

457 (33) Gan, M. L.; Zhang, Y. L.; Lin, S.; Liu, M. T.; Song, W. X.; Zi, J. C.; Yang, Y. C.; Fan, X. N.;
458 Shi, J. G.; Hu, J. F.; et al. Glycosides from the root of *Iodes cirrhosa*. *J. Nat. Prod.* **2008**, *71*,
459 647−654.
460 (34) Huo, C. H.; Liang, H.; Zhao, Y. Y.; Wang, B.; Zhang, Q. Y. Neolignan glycosides from
461 *Symplocos caudata*. *Phytochemistry* **2008**, *69*, 788−795.
462 (35) Lee, D. Y.; Song, M. C.; Yoo, K. H.; Bang, M. H.; Chung, I. S.; Kim, S. H.; Kim, D. K.; Kwon,
463 B. M.; Jeong, T. S.; Park, M. H.; et al. Lignans from the fruits of *Cornus kousa* Burg. and their
464 cytotoxic effects on human cancer cell lines. *Arch. Pharm. Res.* **2007**, *30*, 402−407.
465 (36) Miki, K.; Takehara, T.; Sasaya, T.; Sakakibara, A. Lignans of *Larix leptolepis*. *Phytochemistry*
466 **1980**, *19*, 449−453.
467 (37) Xu, Y.; Gu, X.; Yuan, Z. Lignan and neolignan glycosides from the roots of *Glehnia littoralis*.
468 *Planta Med.* **2010**, *76*, 1706−1709.
469 (38) Yoshizawa, F.; Deyama, T.; Takizawa, N.; Usmanghani, K.; Ahmad, M. The constituents of
470 *Cistanche tubulosa* (Schrenk) Hook. f. II. Isolation and structures of a new phenylethanoid glycoside
471 and a new neolignan glycoside. *Chem. Pharm. Bull.* **1990**, *38*, 1927−1930.
472 (39) Tong, X. G.; Cheng, Y. X. Chemical constituents from *Acorus tatarinowii*. *Nat. Prod. Res. Dev.*
473 **2011**, *23*, 404−409.
474 (40) Gangar, M.; Ittuveetil, A.; Goyal, S.; Pal, A.; Harikrishnan, M.; Nair, V. A. *Anti* selective
475 glycolate aldol reactions of (*S*)-4-isopropyl-1-[(*R*)-1-phenylethyl] imidazolidin-2-one: application
476 towards the asymmetric synthesis of 8-4′-oxyneolignans. *RSC Adv.* **2016**, *6*, 102116−102126.
477 (41) Jeong, E. J.; Cho, J. H.; Sung, S. H.; Kim, S. Y.; Kim, Y. C. Inhibition of nitric oxide
478 production in lipopolysaccharide-stimulated RAW264. 7 macrophage cells by lignans isolated from

Euonymus alatus leaves and twigs. *Bioorg. Med. Chem. Lett.* **2011**, *21*, 2283−2286.

(42) Su, S.; Wink, M. Natural lignans from *Arctium lappa* as antiaging agents in *Caenorhabditis elegans*. *Phytochemistry* **2015**, *117*, 340−350.

(43) Hamerski, L.; Bomm, M. D.; Silva, D. H. S.; Young, M. C. M.; Furlan, M.; Eberlin, M. N.; Castro-Gamboa, I.; Cavalheiro, A. J.; Bolzani, V. S. Phenylpropanoid glucosides from leaves of *Coussarea hydrangeifolia* (Rubiaceae). *Phytochemistry* **2005**, *66*, 1927–1932.

(44) Floegel, A.; Kim, D. O.; Chung, S. J.; Koo, S. I.; Chun, O. K. Comparison of ABTS/DPPH assays to measure antioxidant capacity in popular antioxidant-rich US foods. *J. Food Compos. Anal.* **2011**, *24*, 1043−1048.

501

502

503

504

505

506

507

508

509

510

511

512 **Figure Captions**

513 **Figure 1**. Structures of compounds **1**–**18** and **7a**–**9a**.

514 **Figure 2**. Key ^{1}H-^{1}H COSY, HSQC-TOCSY, HMBC and NOESY correlations for compounds **1**, **3**, **7**,

515 **10**.

Table 1. ^{1}H NMR Data of Compounds 1–6[a]

Position	1	2	3	4	5	6
2	6.68 (s)	6.64 (s)	6.63 (s)	6.95 (d, 2.0)	6.97 (d, 1.9)	6.96 (d, 1.7)
5				7.06 (d, 8.5)	6.74 (d, 8.2)	7.08 (d, 8.5)
6	6.68 (s)	6.64 (s)	6.63 (s)	6.67 (dd, 8.5, 2.0)	6.79 (dd, 8.2, 1.9)	6.75 (dd, 8.5, 1.4)
7	5.50 (d, 6.6)	5.49 (d, 6.7)	5.47 (d, 6.5)	5.47 (d, 6.1)	5.47 (d, 7.1)	5.45 (d, 6.4)
8	3.50 (m)	3.45[b]	3.41[b]	3.37 (m)	3.58 (m)	3.37 (m)
9	3.75 (m)	3.73 (m)	3.71 (m)	3.69[b]	3.95 (dd, 9.8, 7,7)	3.71 (m)
	3.66 (m)	3.65 (m)	3.65 (m)	3.62 (m)	3.73 (m)	3.60 (m)
2'	6.97 (br.s)	6.96 (s)	6.95 (s)	6.96 (s)	6.84 (br.s)	6.71 (br.s)
6'	6.97 (br.s)	6.96 (s)	6.96 (s)	6.96 (s)	6.73 (br.s)	6.72 (br.s)
7'	6.57 (d, 15.9)	6.57 (d, 16.0)	6.57 (d, 15.9)	6.57 (d, 15.8)	2.58 (t, 7.6)	2.58 (t, 7.3)
8'	6.22 (dt, 15.9, 6.0)	6.21 (dt, 16.0, 6.0)	6.22 (dt, 15.9, 6.0)	6.21 (dt, 15.8, 5.9)	1.80 (m)	1.79 (m)
9'	4.40 (dd, 13.6, 6.0)	4.41 (dd, 14.0, 6.0)	4.40 (dd, 13.5, 6.0)	4.41 (dd, 13.7, 5.9)	3.79 (m)	3.79 (m)
	4.18 (dd, 13.6, 6.0)	4.18 (dd, 14.0, 6.0)	4.17 (dd, 13.5, 6.0)	4.19 (d, 13.7, 5.9)	3.43 (m)	3.41 (m)
1''	4.21 (d, 7.9)	4.21 (d, 7.8)	4.21 (d, 7.9)	4.21 (d, 7.8)	4.12 (d, 7.8)	4.11 (d, 7.8)
2''	3.00 (m)	3.00 (t-like, 8.4)	3.00 (t-like, 8.7)	3.00 (t-like, 8.3)	2.99[b]	2.97 (m)
3''	3.09 (m)	3.08 (m)	3.09 (m)	3.09 (m)	3.09[b]	3.07 (m)
4''	3.06 (m)	3.07 (m)	3.06 (m)	3.07 (m)	3.06[b]	3.05 (m)
5''	3.15 (m)	3.15 (m)	3.15 (m)	3.15 (m)	3.14[b]	3.14 (m)
6''	3.69 (m)	3.69 (m)	3.69 (m)	3.69[b]	3.67[b]	3.66 (m)
	3.45 (m)	3.45[b]	3.45 (m)	3.46 (dd, 11.5, 5.8)	3.44[b]	3.44 (m)
1'''	4.91 (d, 7.3)	4.88 (d, 6.8)	4.89 (d, 7.1)	4.96 (d, 7.1)	4.24 (d, 7.8)	4.97 (d, 7.3)
2'''	3.20[b]	3.38 (m)	3.41[b]	3.25[b]	2.99[b]	3.31[b]
3'''	3.04 (m)	3.26[b]	3.26[b]	3.25[b]	3.09[b]	3.31[b]
4'''	3.14 (m)	3.26[b]	3.26[b]	3.24 (m)	3.06[b]	3.26 (m)
5'''	3.20[b]	3.26[b]	3.26[b]	3.74 (m)	3.14[b]	3.71 (m)
6'''	3.59 (m)	4.45 (br.d, 11.8)	4.47 (dd, 11.9, 2.1)	4.57 (br.d, 11.6)	3.67[b]	4.55 (br.d, 11.8)
	3.41 (m)	4.15 (dd, 11.8, 6.3)	4.19 (dd, 11.9, 5.9)	4.19 (dd, 11.6, 6.8)	3.44[b]	4.16 (dd, 11.8, 7.0)
2''''		7.36 (d, 2.0)	7.13 (s)	7.19 (s)		7.42 (d, 1.8)
5''''		6.86 (d, 8.5)				6.89 (d, 8.3)
6''''		7.33 (dd, 8.5, 2.0)	7.13 (s)	7.19 (s)		7.46 (dd, 8.3, 1.8)
3/5-OMe	3.74 (s)	3.66 (s)	3.66 (s)	3.72 (s)	3.75 (s)	3.73 (s)
3'-OMe	3.82 (s)	3.81 (s)	3.81 (s)	3.81 (s)	3.77 (s)	3.78 (s)
3''''/5''''-OMe		3.78 (s)	3.76 (s)	3.76 (s)		3.79 (s)

[a] ^{1}H NMR data (δ) were measured at 600 MHz in DMSO-d_6. Proton coupling constants (J) in Hz were given in parentheses. The assignments were based on ^{1}H-^{1}H COSY, NOESY, HSQC-TOCSY, HSQC, and HMBC experiments. [b] Overlapped with other signals.

Table 2. ^{1}H NMR Data of Compounds 7–11[a]

Position	7	8	9	10	11
2	7.10 (d, 1.9)	7.15 (d, 1.9)	7.13 (d, 1.8)	7.00 (d, 1.9)	6.97 (d, 1.9)
5	7.09 (d, 8.3)	7.14 (d, 8.2)	7.12 (d, 8.2)	6.66 (d, 8.0)	6.68 (d, 8.0)
6	6.95 (dd, 8.3, 1.9)	6.99 (dd, 8.2, 1.9)	6.98 (dd, 8.2, 1.8)	6.78 (dd, 8.0, 1.9)	6.76 (dd, 8.0, 1.9)
7	4.86 (d, 5.9)	4.96 (d, 5.1)	4.94 (d, 5.2)	4.70 (t-like, 5.0)	4.71 (t-like, 4.5)
8	4.38 (m)	4.36 (m)	4.34 (m)	4.47 (m)	4.44 (m)
9	3.85[b]	3.79 (dd, 11.9, 4.3)	3.77 (dd, 11.9, 4.4)	3.65 (m)	3.60 (m)
	3.78 (dd, 11.9, 3.7)	3.52 (dd, 11.9, 5.5)	3.50 (dd, 11.9, 5.5)	3.62 (m)	3.29 (m)
2'	7.00 (br.s)	7.07 (d, 2.3)	7.05 (d, 1.6)	7.30 (d, 1.9)	7.35 (d, 2.0)
5'	6.87 (br.s)	6.98 (d, 8.3)	6.97 (d, 8.3)	7.07 (d, 8.5)	7.11 (d, 8.3)
6'	6.87 (br.s)	6.93 (dd, 8.3, 2.3)	6.91 (dd, 8.3, 1.6)	7.20 (dd, 8.5, 1.9)	7.23 (dd, 8.3, 2.0)
7'	6.54 (dt, 15.7, 1.4)	6.57 (dt, 16.0, 1.5)	6.55 (br.d, 15.7)	7.60 (d, 15.8)	7.62 (d, 15.8)
8'	6.18 (dt, 15.7, 6.1)	6.22 (dt, 16.0, 6.3)	6.20 (dt, 15.7, 6.3)	6.76 (dd, 15.8, 7.8)	6.78 (dd, 15.8, 7.9)
9'	4.06 (dd, 6.1, 1.4)	4.09 (dd, 6.3, 1.5)	4.06 (br.d, 6.3)	9.60 (d, 7.8)	9.61 (d, 7.9)
1"	4.81[b]	4.87 (d, 7.3)	4.86 (d, 7.1)		
2"	3.47 (m)	3.50 (m)	3.48 (m)		
3"	3.38[b]	3.4[b]	3.39[b]		
4"	3.38[b]	3.4[b]	3.39[b]		
5"	3.45 (m)	3.48 (m)	3.46 (m)		
6"	3.85[b]	3.88 (m)	3.86 (br.d, 12.1)		
	3.69 (dd, 11.9, 4.9)	3.71 (dd, 12.0, 5.1)	3.69 (dd, 12.1, 3.8)		
3-OMe	3.81 (s)	3.85 (s)	3.83 (s)	3.73 (s)	3.73 (s)
3'-OMe	3.80 (s)	3.88 (s)	3.87 (s)	3.77 (s)	3.83 (s)
9'-OMe	3.36 (s)	3.38 (s)	3.36 (s)		

[a] ^{1}H NMR data (δ) were measured at 600 MHz in CD_3OD for **7**–**9** and DMSO-d_6 for **10**, **11**. Proton coupling constants (J) in Hz were given in parentheses. The assignments were based on NOESY, HSQC, and HMBC experiments. [b] Overlapped with other signals.

Table 3. ^{13}C NMR Data of Compounds 1–6

Position	1	2	3	4	5	6
1	136.9	137.4	137.4	135.3	132.0	135.6
2	104.3	104.0	104.1	110.2	110.5	110.2
3	152.7	152.9	152.8	148.8	147.5	148.9
4	134.2	133.9	134.1	146.1	146.3	146.0
5	152.7	152.9	152.8	114.8	115.2	115.0
6	104.3	104.0	104.1	117.7	118.5	117.7
7	87.1	87.1	87.0	86.6	86.7	86.3
8	52.9	53.0	53.0	53.2	50.6	53.5
9	62.9	62.8	62.8	62.9	70.1	63.0
1'	130.3	130.3	130.3	130.2	134.9	134.8
2'	115.2	115.3	115.2	115.3	116.8	116.6
3'	143.7	143.8	143.7	143.7	143.3	143.4
4'	147.3	147.4	147.3	147.3	145.5	145.5
5'	129.3	129.3	129.3	129.3	128.6	128.7
6'	110.6	110.6	110.6	110.5	112.7	112.6
7'	131.7	131.8	131.8	131.8	31.4	31.4
8'	123.7	123.6	123.6	123.6	31.4	31.4
9'	68.7	68.7	68.7	68.7	68.0	67.9
1"	102.0	102.0	102.0	102.0	102.9	103.0
2"	73.5	73.5	73.5	73.5	73.5	73.5
3"	76.9	76.9	76.9	76.9	76.8	76.8
4"	70.1	70.1	70.1	70.1	70.1	70.1
5"	76.8	76.8	76.8	76.8	76.7	76.7
6"	61.1	61.1	61.1	61.1	61.1	61.1
1"'	102.6	102.7	102.8	99.8	102.8	99.8
2"'	74.1	74.0	74.1	73.1	73.5	73.1
3"'	77.1	76.2	76.1	76.6	76.9	76.6
4"'	69.9	70.0	70.0	70.1	70.1	70.0
5"'	76.5	74.1	74.1	73.9	76.8	73.8
6"'	60.9	63.6	63.8	64.0	61.1	63.9
1""		120.4	119.3	120.0		120.5
2""		112.5	107.0	107.2		112.6
3""		147.4	147.5	147.7		147.4
4""		151.7	140.7	140.3		151.6
5""		115.2	147.5	147.7		115.2
6""		123.4	107.0	107.2		123.5
7""		165.4	165.4	165.5		165.4
3/5-OMe	56.5	56.3	56.4	55.7	55.6	55.7
3'/5'-OMe	55.8	55.8	55.8	55.7	55.7	55.7
3""/5""-OMe		55.6	56.1	56.1		55.7

Measured in DMSO-d_6 at 150 MHz.

Table 4. ^{13}C NMR Data of Compounds 7–11

Position	7	8	9	10	11
1	137.8	137.4	137.4	132.9	132.8
2	112.8	112.6	112.6	111.5	111.0
3	150.5	150.6	150.6	146.9	147.0
4	147.4	147.4	147.4	145.5	145.5
5	118.7	118.5	118.5	114.5	114.7
6	121.1	120.9	120.9	119.5	119.0
7	73.9	73.6	73.6	71.6	71.1
8	85.9	86.6	86.6	83.4	83.8
9	62.2	61.9	61.9	60.3	60.2
1'	132.7	132.7	132.8	126.6	126.7
2'	111.4	111.4	111.4	111.4	111.3
3'	151.9	151.7	151.7	149.6	149.6
4'	149.1	149.4	149.4	151.2	151.5
5'	117.7	117.7	117.7	114.5	114.4
6'	120.8	120.6	120.6	123.3	123.4
7'	133.7	133.7	133.7	153.5	153.6
8'	125.3	125.3	125.3	126.3	126.4
9'	74.2	74.2	74.2	194.0	194.0
1"	103.1	103.0	102.9		
2"	74.9	74.9	74.9		
3"	78.2	78.2	78.2		
4"	71.4	71.4	71.4		
5"	77.8	77.8	77.8		
6"	62.5	62.5	62.5		
3-OMe	56.7	56.7	56.7	55.4	55.4
3'-OMe	56.5	56.6	56.6	55.7	55.8
9'-OMe	58.1	58.1	58.1		

Measured in CD_3OD for **7–9** and in DMSO-d_6 for **10**, **11** at 150

MHz.

Table 5. α-Glucosidase Inhibitory, Free Radical Scavenging, and Anti-inflammatory Activities of Compounds 1–18

Compound	α-glucosidase inhibition (IC_{50}, μM)	DPPH (IC_{50}, μM)	ABTS (IC_{50}, μM)	NO inhibition (IC_{50}, μM)
1	48.81 ± 3.40^{c}	> 100	> 100	> 100
2	45.36 ± 2.24^{c}	86.49 ± 2.36^{b}	62.24 ± 1.11^{b}	41.10 ± 3.25^{e}
3	32.31 ± 2.11^{e}	70.36 ± 1.62^{e}	58.50 ± 1.41^{c}	54.43 ± 2.46^{c}
4	31.13 ± 1.89^{e}	74.52 ± 1.66^{d}	51.15 ± 0.95^{e}	39.38 ± 2.42^{e}
5	43.44 ± 2.59^{d}	92.17 ± 2.61^{a}	81.74 ± 1.50^{a}	90.43 ± 4.38^{a}
6	25.62 ± 1.59^{f}	79.36 ± 1.80^{c}	54.67 ± 1.14^{d}	31.36 ± 2.25^{f}
7	68.76 ± 2.49^{a}	> 100	> 100	79.38 ± 3.92^{b}
8	67.70 ± 2.85^{a}	> 100	> 100	78.80 ± 2.76^{b}
9	67.65 ± 2.76^{a}	> 100	> 100	79.13 ± 2.79^{b}
10	14.17 ± 1.94^{g}	17.98 ± 0.95^{l}	10.80 ± 0.57^{k}	10.88 ± 1.29^{h}
11	15.56 ± 1.28^{g}	30.56 ± 1.19^{k}	18.65 ± 0.91^{j}	15.50 ± 1.33^{h}
12	66.42 ± 2.40^{a}	> 100	> 100	80.56 ± 4.47^{b}
13	52.88 ± 2.13^{b}	71.58 ± 1.41^{e}	61.47 ± 1.44^{b}	> 100
14	54.63 ± 2.34^{b}	57.45 ± 1.40^{g}	47.48 ± 1.39^{f}	12.54 ± 1.82^{h}
15	42.79 ± 2.59^{d}	40.31 ± 1.09^{j}	27.84 ± 1.05^{i}	> 100
16	41.44 ± 1.91^{d}	61.45 ± 1.43^{f}	42.78 ± 1.15^{g}	> 100
17	33.20 ± 1.93^{e}	51.35 ± 1.09^{h}	33.48 ± 0.99^{h}	32.59 ± 2.38^{f}
18	31.63 ± 2.02^{e}	46.42 ± 1.35^{i}	31.60 ± 1.06^{h}	21.10 ± 1.82^{g}
Acarbose	15.41 ± 0.68^{g}			
Trolox		38.68 ± 1.24^{j}	26.30 ± 1.26^{i}	
Indomethacin				49.46 ± 2.67^{d}

Values were represented as mean ± SD (n = 3). The values were expressed with the different superscript letters in the same column differ significantly (one-way ANOVA and Duncan's test, $p < 0.05$).

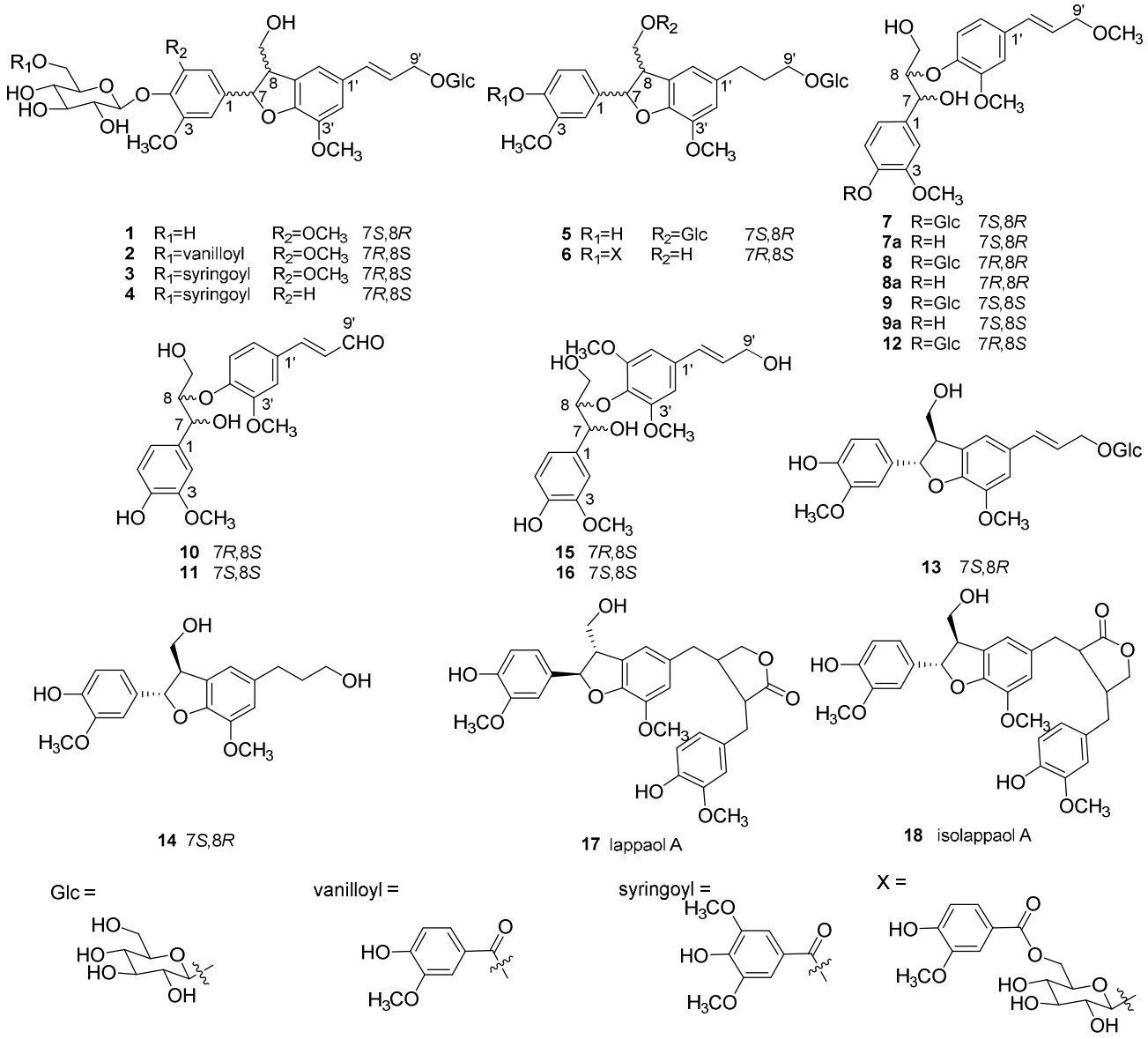
1 R1=H R2=OCH3 7S,8R
2 R1=vanilloyl R2=OCH3 7R,8S
3 R1=syringoyl R2=OCH3 7R,8S
4 R1=syringoyl R2=H 7R,8S
5 R1=H R2=Glc 7S,8R
6 R1=X R2=H 7R,8S
7 R=Glc 7S,8R
7a R=H 7S,8R
8 R=Glc 7R,8R
8a R=H 7R,8R
9 R=Glc 7S,8S
9a R=H 7S,8S
12 R=Glc 7R,8S
10 7R,8S
11 7S,8S
15 7R,8S
16 7S,8S
13 7S,8R
14 7S,8R
17 Iappaol A
18 isolappaol A
Glc =
vanilloyl =
syringoyl =
X =

Figure 1

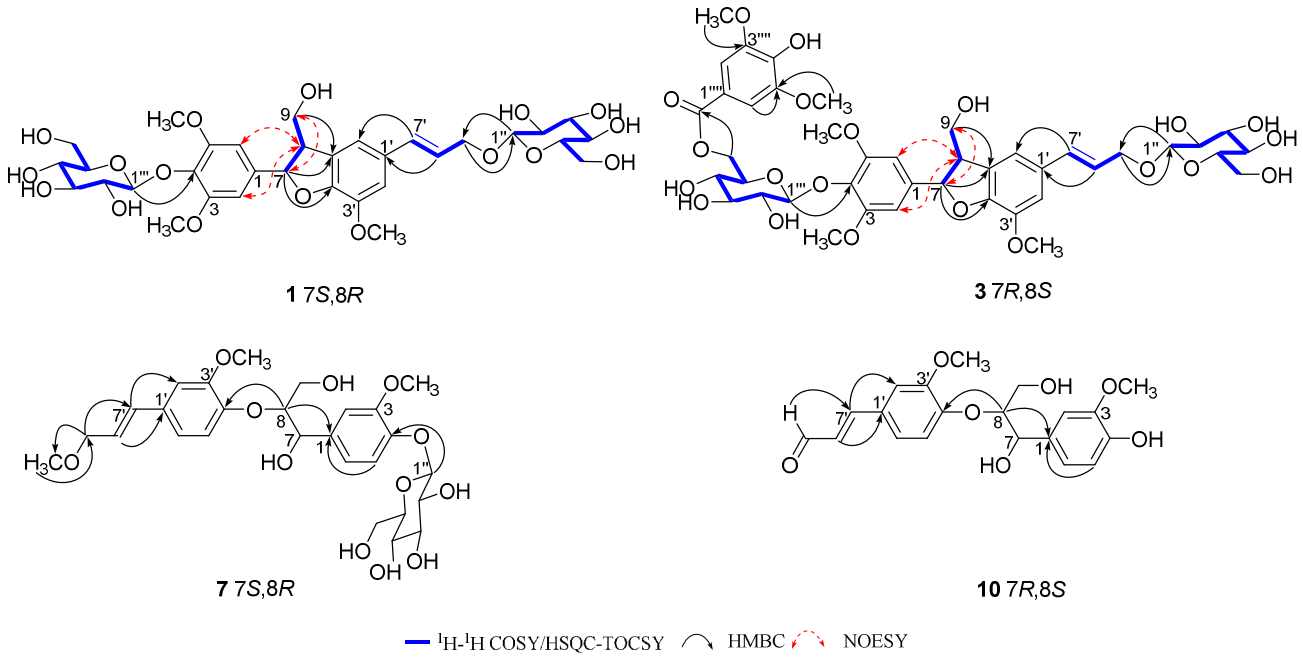

Figure 2

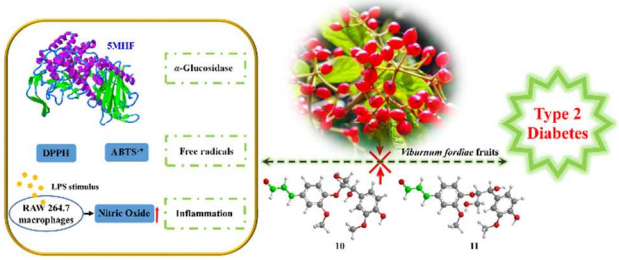

Table of Contents Graphic